Isothermal Thickening and Thinning Processes in Low-Molecular-Weight Poly(ethylene oxide) Fractions Crystallized from the Melt. 8. Molecular Shape Dependence[§]

Er-Qiang Chen, Song-Wook Lee, Anqiu Zhang, Bon-Suk Moon, Ian Mann, Frank W. Harris, and Stephen Z. D. Cheng*

Maurice Morton Institute and Department of Polymer Science, The University of Akron, Akron, Ohio 44325-3909

Benjamin S. Hsiao and Fengji Yeh

Department of Chemistry, The State University of New York at Stony Brook, Stony Brook, New York 11794-3400

Ernest von Merrewell

Department of Physics, The University of Akron, Akron, Ohio 44325

David T. Grubb

Department of Materials Science and Engineering, Cornell University, Ithaca, New York 14853

Received January 7, 1999; Revised Manuscript Received May 5, 1999

ABSTRACT: Three- and four-arm poly(ethylene oxide) (PEOs) fractions have been synthesized to investigate the molecular shape dependence on polymer crystallization, melting, and annealing behaviors. Each arm in these star PEOs has a molecular weight (MW) of 2220 (M_a = 2220) and has been coupled using 1,3,5-benzene tricarbonyl trichloride and 1,2,4,5-benzene tetracarboxylic acid. Molecular parameters have been characterized via vapor pressure osmometry, gel permeation chromatography, light scattering, and Fourier transfer infrared spectroscopy. The coupling agents containing phenylene groups act as chemical defects at the center of the molecule. Diffusion in the melt of these star PEOs as measured by nuclear magnetic resonance shows that at constant temperature the self-diffusion slows down with an increase in the number of arms. Wide-angle X-ray diffraction (WAXD) experiments indicate that these star PEOs possess monoclinic crystal structures identical to those of linear PEOs, implying that the coupling agents are rejected from the crystals. The overall crystallization rate of the star PEOs decreases with increasing crystallization temperature (T_c) and number of arms. On the basis of synchrotron small-angle X-ray scattering (SAXS) experiments, it has been found that during the initial isothermal crystallization at low undercoolings (ΔT's) the long period gradually decreases with increasing time before reaching a thickness corresponding to the summation of the thicknesses of the crystals with an extended arm length and two layers consisting of the coupling agent and the uncrystallized PEO arm. The final crystals possess the regular overall molecular conformations. At high ΔT's, the long period remains constant both during and after crystallization with no observed thinning process. Only irregular overall molecular conformations in these crystals can be expected. The dependence of the final long period on T_c, as determined by SAXS, is remarkably similar to the melting temperature response to T_c obtained via differential scanning calorimetry (DSC). The annealing effect has been examined for samples crystallized at 32 °C, subsequently heated to 50 °C, and isothermally annealed for various periods of time. A partial melting upon heating and recrystallization during annealing can be identified based on the combined experimental results obtained from DSC, WAXD, and SAXS methods.

Introduction

The crystallization of polymers has been an important topic in polymer physics for the past several decades. Chain folding in polymer lamellar crystals is the key mechanism which distinguishes polymer crystallization and morphology from that of small molecules. During the 1960−1970s, a series of crystallization, melting, and morphology studies on low-molecular-weight (LMW) poly(ethylene oxide) (PEOs) fractions were reported.[1−11] In the low-undercooling (ΔT) region, LMW PEOs possess integral folding (IF) chain crystals, implying that the end groups (−OH) of these PEOs are rejected from the crystal interior and that hydrogen bonds are formed and located at the lamellar basal surfaces. The folded chain crystals in these PEOs are metastable with respect to the extended chain crystals. It was observed that the lamellar thickness increases in a stepwise manner with decreasing ΔT. Unfolding processes during annealing can also occur through the diffusion motion of the chain along the *c*-axis, wherein the remaining lattice vacancy is replaced by another molecule extracted from the melt.

In our studies, nonintegral folding (NIF) chain crystals can be formed during crystallization as an intermediate stage with respect to the IF crystals.[12−22] Although the NIF crystals are thermodynamically the least stable, they possess the most favorable kinetics, i.e., the nucleation barrier of this NIF crystallization is the lowest.[23,24] Subsequent transformation from the NIF crystal to the more stable IF crystals occurs via thicken-

* To whom the correspondence should be addressed.

[§] For corrections to this paper, see: *Macromolecules* **1999**, *32*, 5174.

10.1021/ma9900176 CCC: $18.00
Published on Web 06/18/1999

ing and thinning processes. Further research was also carried out to understand the different effects on the LMW PEO crystallization, such as the MW dependence[18] and chain end effects.[19]

Recently, three two-arm PEOs were prepared using a coupling reaction. These PEOs had the same number average MW (M_n) of 2220 for each arm. The coupling agents used were *para*-1,4-, *meta*-1,3-, and *ortho*-1,2-benzene dicarbonyl dichlorides, and therefore at the molecular centers, the configurations of these two-arm PEOs exhibited angles of 180°, 120°, and 60°, respectively. These coupling agents may substantially affect the overall molecular conformations (simply abbreviated to be conformations in this study) in the crystals of the two-arm PEOs.[20−22] Wide-angle X-ray diffraction (WAXD) patterns indicated that these fractions have the same crystal structure regardless of the coupling agents (which act as chemical or configurational defects) used, implying that the defects must be excluded from the crystals. Differential scanning calorimetry (DSC) results demonstrated that two populations of crystals existed when the samples were crystallized at low ΔT's particularly in the cases of the 1,4- and 1,3-two-arm PEOs. The corresponding small-angle X-ray scattering (SAXS) experiments showed two different long periods in these fractions. It is understood that the crystals, which possess the thinner long period, exhibit an extended conformation with a single layer of defects existing between neighboring lamellae. The crystals exhibiting a thicker long period possess a once-folded conformation, with two layers of defects lying between neighboring lamellae.[20−22]

In addition to our two-arm PEO study of polymer crystallization, we have also synthesized three- and four-arm PEOs via coupling reactions. The molecules of these two star PEOs are no longer linear in shape. The arms of the three-arm PEO molecule are connected to the phenylene groups of the coupling agents at the 1, 3, and 5 positions. In the four-arm PEO, the four arms are connected to the phenylene groups of the coupling agents at the 1, 2, 4, and 5 positions. It is expected that the coupling agents are excluded from the crystalline region, due to their bulky size and dissimilarity with respect to the PEO repeating unit.

There are many possible conformations of the star molecules to locate the defects in the amorphous layer and pack the arms in the crystals. In regular conformations of these star PEOs, the arms may be distributed either in two neighboring lamellae or in the same lamella adjacently. Another possible arrangement is for one arm (or even two arms) to remain in the amorphous layer. However, this arrangement must substantially decrease crystallinity of the samples. In this publication, we report the crystallization, melting, and annealing behaviors of the star PEOs and try to understand the effect of molecular shape.

Experimental Section

Material Synthesis. An α,ω-methoxy-hydroxy poly(ethylene oxide), $HO-(CH_2CH_2O)_n-CH_3$, with M_n = 2220 was purchased (Aldrich). This PEO possesses one hydroxy and one methoxy end groups. Further fractionations were carried out in our laboratory. Coupling agents of 1,3,5-benzene tricarbonyl trichloride and 1,2,4,5-benzene tetracarboxylic acid were also purchased from Aldrich and were used to prepare three- and four-arm PEOs, respectively. For the three-arm PEOs, the synthesis and fractionation procedures are identical to that of two-arm PEOs reported previously.[20−22] To synthesize the four-arm PEO, a strong dehydrant, 1,3-dicyclohexylcarbodiimide (DCC), was required to act as a reactant. A 20 g fraction of linear PEO (M_n = 2220) and a slightly less than stoichiometric amount of 1,2,4,5-benzene tetracarboxylic acid were dissolved in tetrahydrofuran (THF) with an excess of DCC. The reaction mixture was vigorously stirred and kept at 25 °C for 2 days under a nitrogen atmosphere. After the reaction, purification and fractionation of the PEOs were conducted by the nonsolvent addition to remove the linear "parent" PEOs and the star polymers of lower arm numbers. Figure 1 denotes the reactions for both the three- and four-arm PEOs.

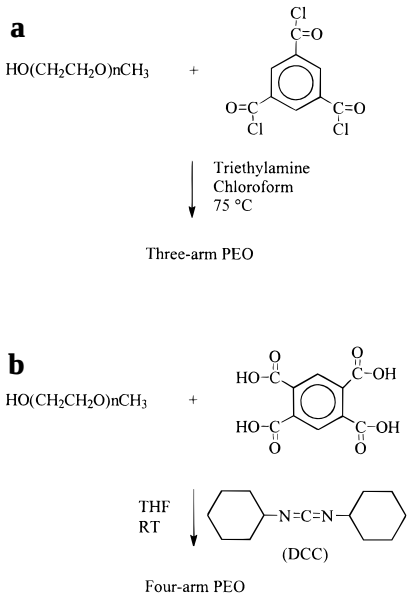

Figure 1. Schematic diagram of the synthesis of (a) three- and (b) four-arm star PEOs.

Equipment and Experiments. Gel permeation chromatography (GPC) coupled with viscometry and light scattering was employed to characterize the MW, MW distribution, and the radius of gyration of the star PEO molecules. The GPC experiments were carried out in THF at 30 °C. Four μ-styragel columns were used with pore sizes of 10, 50, 100 and 1 000 nm. The effective MW range for the columns was 500−600 000. Standard linear PEO fractions in the same MW range were used for GPC calibration. Knauer vapor pressure osmometer (VPO) was also applied for determining the number-average MW in toluene at 40 °C. Fourier transfer infrared spectroscopy (FTIR, Mattson Galaxy 5020) measurements were carried out over a spectrum ranging from 500 to 4000 cm^{-1} to analyze the end groups and coupling agents.

Self-diffusion coefficients of these star PEOs in the melt were determined by a pulsed-gradient spin−echo (PGSE) nuclear magnetic resonance (NMR) method.[25] The molecular mobility of PEOs in the melt was investigated using proton NMR at 33 MHz using a spin-lock CPS-2 spectrometer with a Varian high-impedance current-regulated electromagnet. The principal echo on-resonance without Fourier transform was measured using radio frequency phase-sensitive detection. Its attenuation in the presence of a pair of applied magnetic field gradient pulses was also detected. For the star samples, measurements at three temperatures (60.5, 80.5, and 100.5 °C) were conducted.

Differential scanning calorimetry (TA2100) experiments were carried out to study the isothermal crystallization, melting, and annealing behavior of the star PEOs. The DSC was calibrated using indium and other standard materials with a precision of ±0.2 °C. The samples were encapsulated in hermetically sealed aluminum pans. The sample weight used was approximately 0.5 mg, and the pan weights were kept constant. Isothermal crystallization was performed by quenching from the isotropic melt to the preset crystallization temperature (T_c) for different crystallization times (t_c's). In the low ΔT range, a self-seeding technique was used for the

isothermal crystallization.[7] After being annealed at a selected self-seeding temperature T_s ($T_m - T_s \approx 1.5$ °C) for 20 min, the samples were shifted to the preset T_c. The samples were then heated above the melting temperature (T_m) with a heating rate of 5 °C/min, and the melting traces were recorded after the completion of crystallization.

Real-time synchrotron simultaneous WAXD and SAXS experiments were carried out at the synchrotron X-ray beam line 27C of the National Synchrotron Light Source at Brookhaven National Laboratory. The collimation geometry used has been described by Chu et al.[26] The position-sensitive proportional counters were used to record the scattering patterns. The counter of SAXS was calibrated with a duck tendon giving scattering vectors (q) of 0.0109, 0.022, 0.033 nm^{-1} and so on ($q = 4\pi \sin\theta/\lambda$, where λ is the wavelength of the X-ray radiation). Isothermal crystallization and annealing measurements were made on a customized two-chamber hot stage. The temperature was controlled within ±0.3 °C. Lorentz correction was conducted by multiplying the intensity, I (counts per second), by q^2. The relative invariant Q' was calculated based on an integration of $\int(I - I_b)q^2\,dq$,[27] where this integration covered q's ranging from 0.08 to 0.2 nm^{-1} and I_b is the intensity of PEO liquid scattering obtained using the Porod's law extrapolation. WAXD and SAXS experiments were also carried out in our laboratory. Rigaku 12 and 18 kV rotating-anode generators were utilized for WAXD and SAXS, respectively. The WAXD patterns were recorded on a D/max-B X-ray diffractometer using a pulse-height analyzer. The SAXS patterns were recorded on a position-sensitive detector.

A thermal history of annealing experiments was determined by following a specific procedure; i.e., the samples were quenched from the isotropic melt and isothermally crystallized at 32 °C for 30 min to reach the maximum crystallinity, followed by heating to 50 °C at a heating rate of 3 °C/min. Once 50 °C was reached, the samples were held for different annealing times (t_a's) to monitor the annealing effect on the long period, crystallinity, and T_m. This procedure was carried out in DSC, WAXD, and SAXS experiments.

Results and Discussion

Molecular Characterization. Figure 2 represents the GPC diagrams for the linear "parent" PEO and the unfractionated and fractionated four-arm PEOs. It is evident that the unfractionated four-arm PEO contains the linear "parent" PEO component. After multiple step fractionations, the GPC diagram of this four-arm PEO shows that the MW distribution is unimodal and narrow. The fractionated three-arm PEO exhibits a similar MW distribution. The number- and weight-average MWs obtained from the different characterization methods are listed in Table 1. The mean-square radii of gyration of the linear "parent" and the star PEOs calculated based on the light scattering experiments are also included. On the basis of a random flight model of star molecules, a theoretical expression[28,29] for the ratio of the mean-square radii of gyration between a star molecule with identified arms and an individual arm can be written as

$$\langle R_g^2\rangle_s/\langle R_g^2\rangle_a = (3p - 2)/p \qquad (1)$$

where p is the number of the arms and $\langle R_g^2\rangle_s$ and $\langle R_g^2\rangle_a$ are the mean-square radii of gyration of the star molecule and the individual arm, respectively. From Table 1, the ratios obtained from the experiments are close to the calculated theoretical values using eq 1.

The end groups of the linear "parent" and the star PEOs have been examined via FTIR, and the results are presented in Figure 3. In the case of the linear PEO, a broad vibration band occurs at 3500 cm^{-1}, originating from the strong hydrogen bonding and −OH stretching.

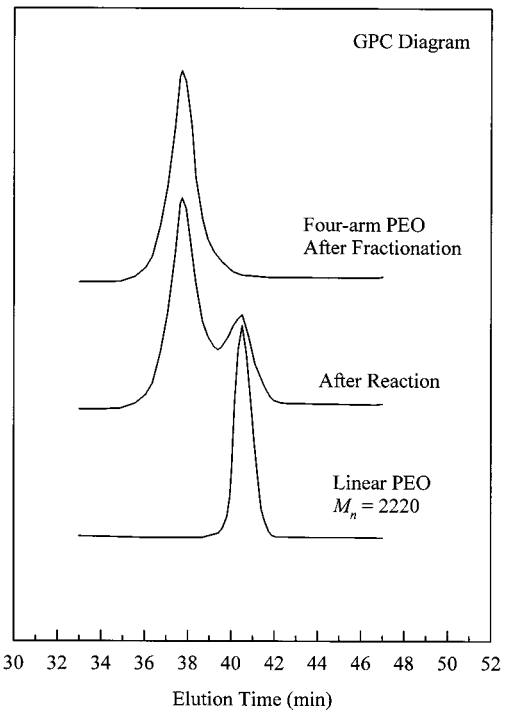

Figure 2. Gel permeation chromatogram of the linear "parent" PEO and the unfractionated and fractionated four-arm star PEOs.

Table 1. Molecular Characteristics of Linear and Star PEO Fractions

	M_n[a]	M_n[b]	M_w/M_n[c]	$\langle R_g^2\rangle_s$ (nm^2)[d]	$\langle R_g^2\rangle_s/\langle R_g^2\rangle_a$
linear PEO (arm)	2200	2220	1.02	4.04	
three-arm PEO	6800	6700	1.08	9.48	2.3,[e] 2.3[f]
four-arm PEO	8900	8600	1.12	10.6	2.6,[e] 2.5[f]

[a] Number-average molecular weight measured from GPC coupled with viscometry and light scattering experiments. [b] Number-average molecular weight obtained from VPO. [c] Polydispersities measured from GPC coupled with viscometry and light scattering experiments. [d] Mean-square radius of gyration obtained from light scattering experiments. $\langle R_g^2\rangle_s$ and $\langle R_g^2\rangle_a$ are the mean-square radii of gyration of the star molecules and the individual arm, respectively. [e] Measured results using light scattering experiments. [f] Theoretical results calculated using eq 1.

Since the linear PEO has only one −OH end group, the hydrogen bond formed should be intermolecular. No such vibration band appears in the star PEOs due to their $-CH_3$ end groups. Moreover, the star PEOs show the 1720 cm^{-1} vibration band, which corresponds to the ketone (−C═O) stretching vibration resulting from the coupling agent at the center of the star PEO molecules.

WAXD results for the linear and the star PEOs show identical diffraction peak positions (see below), indicating that the molecular shape does not affect the monoclinic PEO crystal structure.[30] Despite the higher PEO segment density at the center of the star molecules and their complex molecular shapes, the star PEOs also exhibit higher degrees of crystallinity after the weight normalization of the coupling agents, and all of them are around 75−85%, nearly 10−20% lower than that of the linear ones.

Self-diffusion coefficients (D) measured at three different temperatures using PGSE-NMR for the three- and four-arm PEOs are illustrated in Figure 4. The D's of the linear "parent" and the three two-arm PEOs are also shown in this figure for comparison. In brief, the

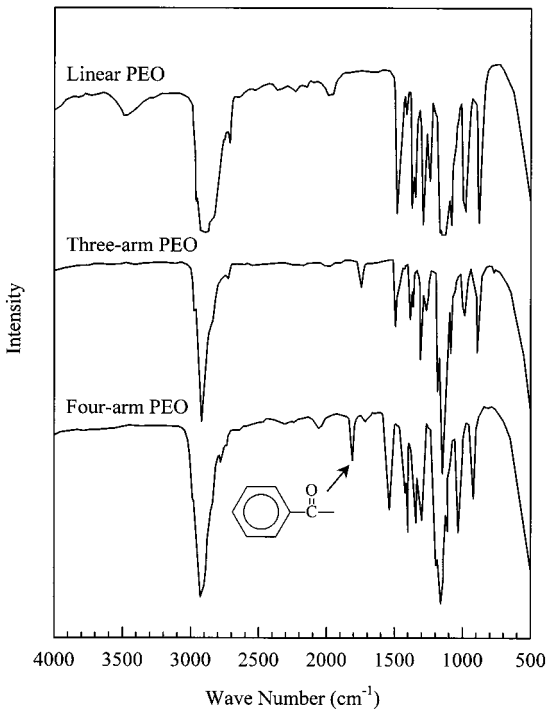

Figure 3. FTIR spectra of the linear and star PEOs with each arm having $M_a = 2220$.

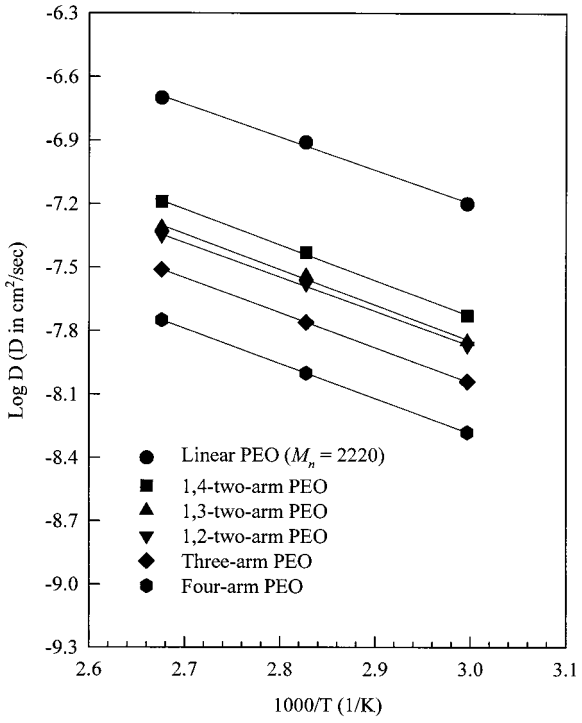

Figure 4. Self-diffusion coefficients as a function of temperature in the melt of the linear and star PEOs with each arm having $M_a = 2220$.

self-diffusion motion slows down when the number of arms increases from two to four. It is apparent that D increases with increasing temperature, which obeys Fick's law. The temperature dependence of D can be described in terms of the Arrhenius equation

$$D(T) = D_0 \exp\{-E_a/kT\} \qquad (2)$$

where E_a is the activation energy for diffusion, D_0 is assumed to be a temperature independent constant, and

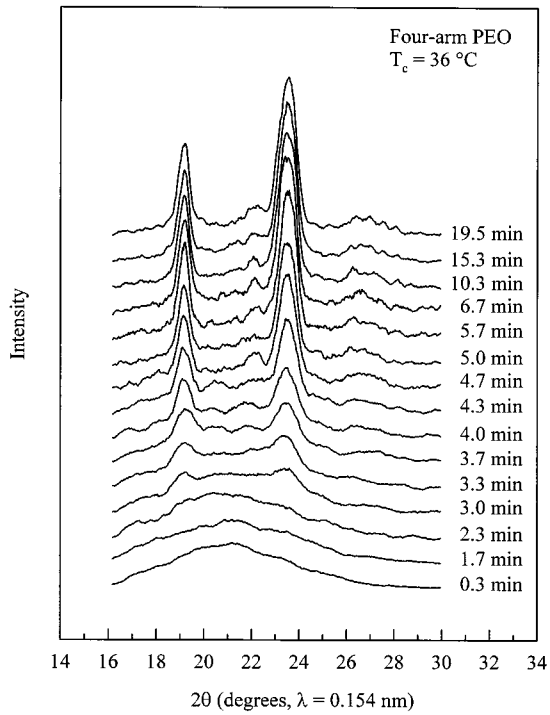

Figure 5. WAXD patterns for the four-arm PEO isothermally crystallized at 36 °C.

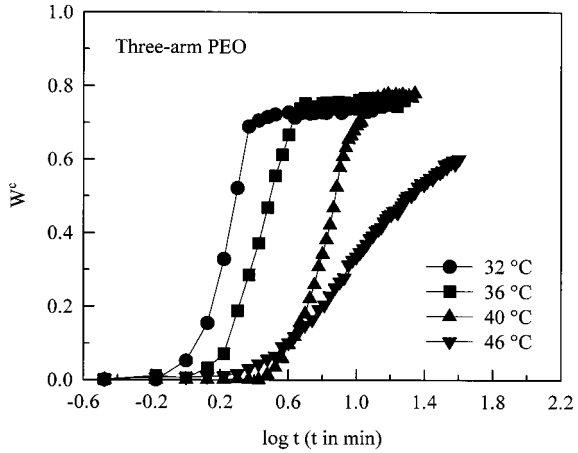

Figure 6. Crystallinity as a function of t_c for the three-arm PEO crystallized at different T_c's.

k is the Boltzmann constant. An E_a of 30 ± 2 kJ/mol can be determined for the linear and star PEOs. Despite the very different molecular shape, these star PEOs possess E_a's similar to those of linear PEOs.[22,31] This indicates that the E_a is primarily dependent upon the mobility of the PEO segments.

Overall Crystallization Kinetics. The isothermal crystallization processes of the three- and four-arm PEOs have been investigated via DSC and simultaneous measurements of real-time WAXD and SAXS. Figure 5 shows the WAXD patterns of the four-arm PEO crystallized at 36 °C. The development of crystallinity can be demonstrated by a decrease of the amorphous halo and an increase of the crystalline reflection intensity with increasing t_c. Figure 6 presents the crystallinity determined by WAXD as a function of t_c for the three-arm PEO crystallized at different T_c's. The overall crystallization rates decrease with increasing T_c. In particular, the crystallization of this star PEO becomes very slow at low ΔT's (such as $T_c = 46$ °C). Even though the self-

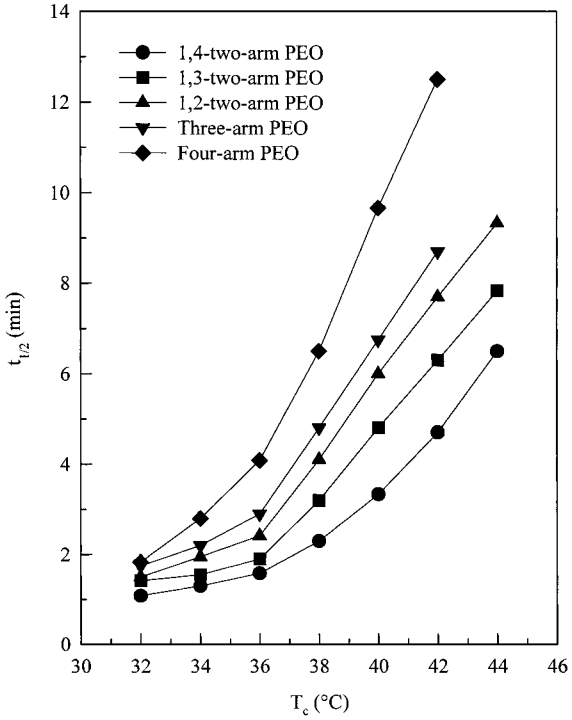

Figure 7. $t_{1/2}$ of the overall crystallization in the two-, three-, and four-arm PEOs at different T_c's.

seeding was utilized to accelerate the crystallization process and the induction period has been sufficiently reduced due to the existence of seeds, the crystal growth rates are still much slower than those at high ΔT's. Figure 7 illustrates that the two-, three- and four-arm PEOs have a relationship of the $t_{1/2}$ with the T_c's obtained from both DSC and WAXD experiments (where the $t_{1/2}$ represents the time required to reach half of the crystallinity during isothermal crystallization). It is evident that the crystallization rate (determined by both primary and surface nucleation processes[32−36]) decreases with an increasing number of arms at the same T_c. This is mainly attributed to the molecular shape which deviates from the linear chain.

Changes of Long Periods and Crystal Morphologies. SAXS experiments illustrate the evolution of crystal morphology of the three- and four-arm PEOs. The real-time SAXS results of the three- and four-arm PEOs crystallized at 40 °C are shown in Figure 8. A broad SAXS peak first appears following the induction period in these two star PEOs. The intensities of the scattering maximum increase with increasing t_c. The second-order scattering gradually develops, manifesting the lamellar morphology of the star PEOs. During the evolution of the scattering intensity, the peak positions shift slightly toward higher q values over a short period of time. This behavior may be recognized as an apparent thinning process. The three-arm PEO has an initial long 19.0 nm at $t_c = 3$ min and decreases to 17.0 nm for t_c exceeding 6 min (Figure 8a). In the case of the four-arm PEO, the long period of the initial peak at $t_c = 5$ min is approximately 20.0 nm and reduces to 17.0 nm when t_c exceeds 8 min (Figure 8b).

This apparent thinning process is, however, strongly dependent on the ΔT. Figure 9 illustrates the long period development during isothermal crystallization at different T_c's for the three-arm PEO. As shown in Figure 8a at intermediate ΔT's such as $T_c = 40$ °C, this star PEO possesses a minor decrease of the long period after

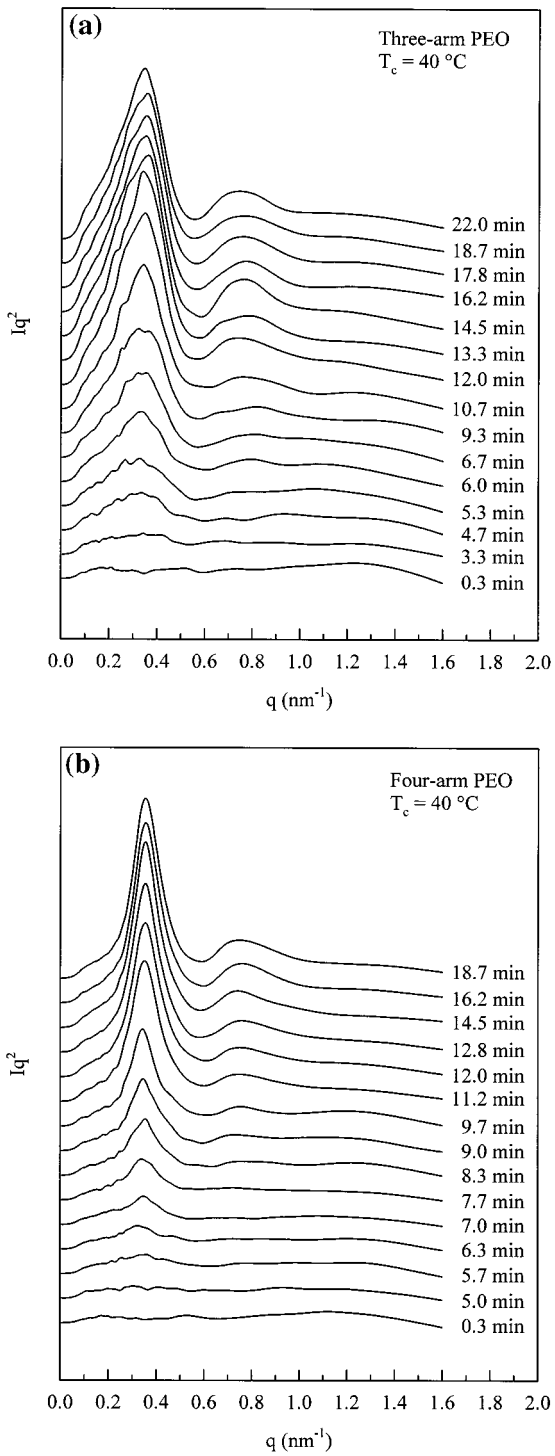

Figure 8. Two sets of SAXS of (a) the three-arm and (b) the four-arm PEOs at $T_c = 40$ °C.

an initial t_c when crystallization takes place. This apparent thinning process cannot be observed at high ΔT's such as $T_c = 32$ °C (when $T_c < 36$ °C), wherein the long period remains constant at 15.2 nm throughout crystallization. However, when the ΔT of the crystallization is low, a thinning process can clearly be seen. For example, the three-arm PEO shows a long period change from approximately 26.5 to 19.0 nm at $T_c = 46$ °C and $t_c = 42$ min. The four-arm PEO also exhibits a similar behavior. Compared with the overall crystallization kinetics, it seems that the slower the crystallization rate the more pronounced the thinning process.

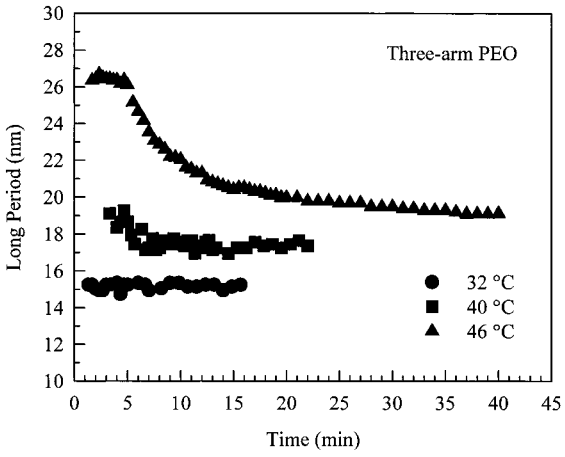

Figure 9. Long period changes with t_c for the three-arm PEOs crystallized at different T_c's.

Figure 10 illustrates the relationship between the long period at the final stage and the T_c for the three- and four-arm PEOs. The long period increases with increasing T_c in both of the star PEOs. Note that the extended chain crystal of the linear PEO ($M_n = 2220$) possesses a long period of 14.8 nm.[20] The crystallinity of the linear PEO can be as high as 95%, corresponding to a lamellar thickness of approximately 14.0 nm. The star PEOs possess long periods of approximately 15 nm for $T_c < 36$ °C. The crystallinity of the star PEOs is nearly 20% lower (after a weight correction for the coupling agents) than that of the linear PEO in this ΔT region. This indicates that the lamellar thickness of the star PEOs is smaller than 14 nm, and thus, the star molecules most likely adopt irregular conformations in the crystals. Note that the bulky coupling agents are not included in the PEO crystal lattice even at the initial stage of crystallization. Moreover, some of the arms may remain in the amorphous layers as a result of the fast crystallization. Therefore, the thickness of the amorphous layers increases, and no thinning process is observed in this T_c region.

Between T_c's of 36 and 44 °C, the long periods of the star PEOs increase by almost 3 nm. The long period gradually reaches a constant for further increase in T_c. The final long period is approximately 19.0 nm for T_c above 46 °C. Comparing the final long period of the star PEOs with that of linear PEO ($M_n = 2220$), a difference of approximately 4 nm can be found. Since the T_m's of the star PEOs in this T_c region are identical or even higher than that of the linear one (see below), one may assume that the crystal lamellae of both the star and the linear PEO are identical. The amorphous layer for the star PEOs is thus as thick as approximately 4 nm and consists of both amorphous PEO and the coupling agent.

First, the size of coupling agents needs to be estimated. If one uses a simple mean-field consideration, the coupling agents for the star PEOs have MWs of 207 (three-arm) and 250 (four-arm), respectively. Assuming a reasonable density of the coupling agents of roughly 1.0 g/cm^3, the volume of the coupling agents should be approximately 0.4 nm^3. Note that the coupling agent possess a length of around 1 nm on the basis of computer simulation.[20−22] Therefore, the cross section of coupling agents is 0.4 nm^2, whereas the cross section of a PEO chain in the crystal is 0.21 nm^2. This indicates that the coupling agents cannot be included in the

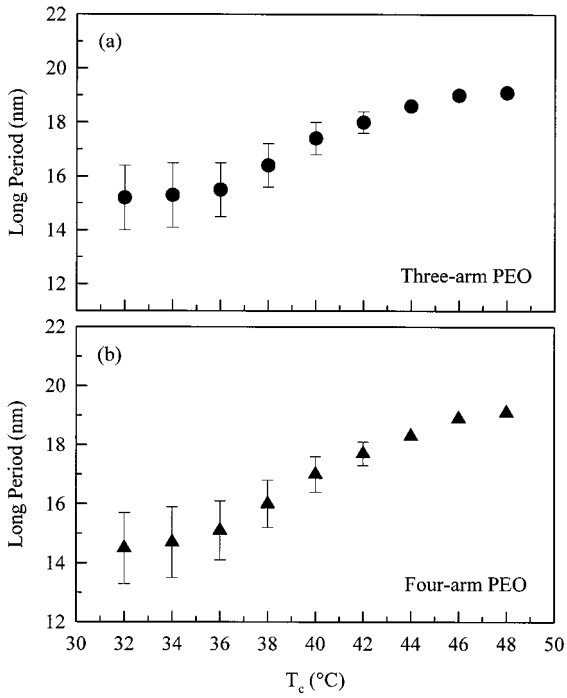

Figure 10. Relationship between the final long period and T_c for both (a) the three- and (b) four-arm star PEOs.

crystal. Furthermore, these defects most likely occupy a certain thickness in the amorphous layers [between 0.6 (the width of the coupling agent) and 1 nm (the length of the coupling agent)].

Second, the amorphous PEO should also contribute to the thickness of this amorphous layer, as evidenced by a 10% − 15% lower crystallinity of the star PEOs (after the weight normalization of the coupling agent) compared to that of the linear one at $T_c = 46$ °C. There exist two possible cases. In the first possibility, all of the amorphous PEO could be made of a small portion of each PEO arm during crystallization. However, this assumption naturally decreases the lamellar crystal thickness due to the fixed arm length, and thus, the T_m of the star PEO crystals must be reduced. This is not found in our experimental observations (see below). The other possibility assumes that all of the amorphous PEO might be attributed to a few completely uncrystallized PEO arms. To match the crystallinity data of 80% − 85%, it would be equivalent to having one arm which is not crystallized for every six arms in the star PEOs (which roughly corresponds to 2 three-arm PEOs or 1.5 four-arm PEOs). These uncrystallized arms must be located in the amorphous layers, and thus, the layer thickness is increased. Using a mean-field consideration to semiquantitatively estimate this part of the contribution to the amorphous layer thickness, one PEO arm occupies a volume of about 3.3 nm^3, assuming the arm is isotropic (the density of amorphous PEO is 1.123 g/cm^3). For each uncrystallized arm in the star PEOs, the cover area on both sides of the lamellar basal surface should be 2.5 nm^2 (0.21 nm^2 × 6 × 2, where 2 represents the two sides of the folded crystal surfaces). This calculation leads to a thickness of 1.3 nm caused by the uncrystallized PEO arms. One may thus conclude that the coupling agents and uncrystallized PEO arms in both sides of the lamellae contribute to the amorphous layers, corresponding to approximately 4 nm.

The remaining issue pertains to the presence of the apparent thinning process during the crystallization. In

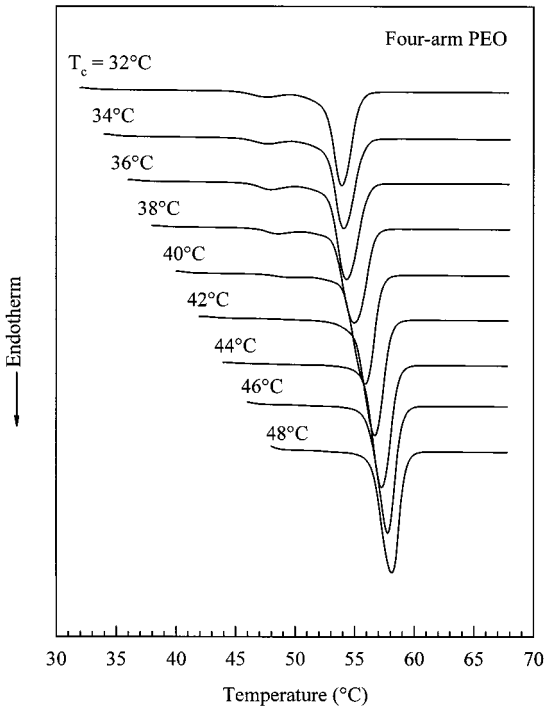

Figure 11. DSC melting traces of the four-arm star PEO crystallized at different T_c's.

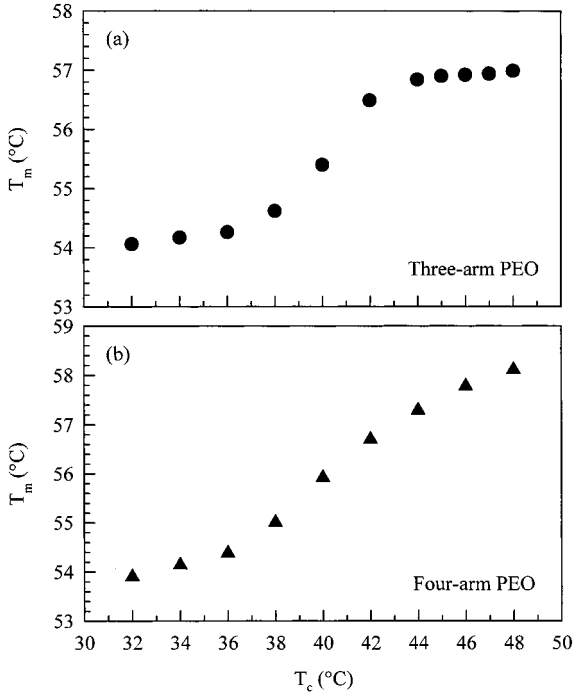

Figure 12. Relationship between T_m and T_c for (a) the three- and (b) four-arm star PEOs.

the initial stage of crystallization at intermediate ΔT's (such as at T_c = 40 °C), the coupling agents are less regularly distributed in the amorphous layers. This leads to thicker amorphous layers and lower crystallinity. As crystallization proceeds, the coupling agents become closely aggregated between two neighboring lamellae, maximizing microphase separation and PEO crystallinity on a local scale. Therefore, thinning of the amorphous layer results in the shift of the observed SAXS peak positions, decreasing in long period. When the crystallization takes place at low ΔT's, the initial long periods for the star PEO crystallization after self-seeding process is rather large (approximately 26.0 nm). Due to the fact that nearly 2−4% of seed crystallinity may remain in the initial stage, the value of 26.0 nm may not truly represent the long period of the star PEO lamellae. The isolated seeds may contribute to the scattering. As crystallization proceeds, the melt between seeds diminishes, which leads to an apparent thinning of the long period.

Melting Behavior of the Crystals with Irregular and Regular Conformations. The crystal melting behaviors of these two star PEOs show that the T_m's are mainly dependent on the MW of each arm and only slightly dependent on the number of the arms. One example is shown in Figure 11 which represents the melting traces of the four-arm PEO crystallized at different T_c's recorded by DSC during heating. At T_c's below 40 °C, there is a low T_m peak which does not exist in linear PEOs, appearing around 45 °C in addition to a major high T_m peak. This small endotherm may be associated with the cooperative motion of PEO chains with the coupling agents, which is evident by a small but sudden increase of the *d* spacing of the (120) crystal planes observed at 44 °C.[21,22] When T_c exceeds 40 °C, the low T_m peak vanishes. A similar observation can be made for the three-arm PEO.

The T_m of the major melting peak is found to be T_c-dependent, as shown in Figure 12 for both the three- and four-arm PEOs. The tendency of T_m to vary with T_c is remarkably similar to the trend of the long period (Figure 10). For T_c < 36 °C, the T_m's remain nearly constant at approximately 54 °C for both of the star PEOs. Above this T_c, the T_m gradually increases. The T_m reaches a plateau of 56.8 °C for T_c's above 44 °C for the three-arm PEO. In the case of the four-arm star PEO, the T_m still tends to increase slightly with a T_m of 58.1 °C for a T_c of 48 °C.

It is intriguing that at T_c > 44 °C the three-arm PEO possesses T_m's higher than that of the 1,3-two-arm PEO crystals with the extended conformation, but it has almost the same T_m's as that of the once-folded conformation crystals of the 1,3-two-arm PEO. For example, at T_c = 48 °C, the T_m of the three-arm PEO is 57.0 °C, whereas the 1,3-two-arm PEO exhibits a T_m of 57.0 °C for crystals with the once-folded conformation.[21,22] This comparison of the T_m's between the three-arm and 1,3-two-arm PEOs may imply that the thermodynamic stability of the three-arm PEO crystals formed at low ΔT's is predominantly dependent on whether the arms pack in the same lamella (folded conformations).

It is also found that the four-arm PEO exhibits higher T_m's at low ΔT's compared with those of the three-arm PEOs, and the T_m's of four-arm PEO are even higher than those of the 1,2-two-arm PEO which possesses the highest T_m among the three two-arm PEOs.[21,22] For example, the T_m of the four-arm PEO is 0.7 °C higher than that of the 1,2-two-arm PEO at T_c = 48 °C (58.1 °C versus 57.4 °C). The phenomenon may be due to a lower entropy of the four-arm PEO in the melt compared with the others, in addition to the folded conformations. However, detailed statistical mechanics analyses are necessary in order to obtain quantitative thermodynamic functions.

Annealing Behavior in These Star PEOs. The star PEO crystals formed at T_c < 36 °C, even for the prolonged t_c (such as days) show no change in either the long period observed in SAXS or the apparent T_m's seen in DSC at a heating rate of 5 °C/min. Three

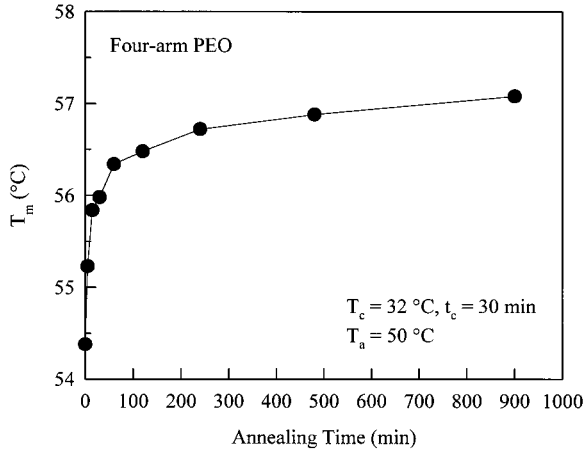

Figure 13. Relationship between T_m and t_a at 50 °C for the four-arm star PEO that was initially isothermally crystallized at 32 °C for 30 min from the isotropic melt.

questions arise: (1) Can the crystals formed at high ΔT's (such as those at 32 °C) be annealed at high temperatures (such as 50 °C) in order to significantly improve the metastability of the crystals? (2) What molecular mechanisms are involved in this annealing process? (3) Are the annealed crystals identical to those crystallized directly from the melt at low ΔT (at 50 °C)? Figure 13 shows the result of the annealing experiment, wherein the four-arm PEO is completely crystallized at 32 °C for 30 min, followed by heating the sample to 50 °C at 3 °C/min and annealing there for different t_a's. The T_m increases from 54.3 °C to 56.7 °C within a t_a of 240 min. The T_m increases to 57.1 °C upon increasing t_a to 900 min. Similar behavior of the annealing process can also be observed in the three-arm PEO, wherein the T_m is 54.3 °C after crystallization at 32 °C and increases to 56.7 °C for t_a = 240 min and 56.9 °C for t_a = 900 min. It is evident that the initial increase of T_m is sudden and is followed by a gradual increase. The overall increase of T_m for the crystals formed at 32 °C after annealing at 900 min at 50 °C is 2.6 °C (54.3 °C versus 56.9 °C) for three two-arm PEOs, whereas the change is 2.8 °C (54.3 °C versus 57.1 °C) for the four-arm PEO. This indicates that annealing the crystals at higher temperatures can improve the stability of the crystals.

The annealing behavior of these two star PEOs has also been investigated using real-time synchrotron SAXS and WAXD. Figure 14 describes the long period (Figure 14a), crystallinity (Figure 14b), and relative invariant Q' (Figure 14c) changes for the three-arm PEO during both heating and annealing. The temperature profile of the experiment is also included in Figure 14c (the solid line). Figure 14a demonstrates an initial long period of approximately 15.0 nm. The long period starts to increase as soon as the temperature reaches 44 °C; finally, this long period plateaus at 19.0 nm after annealing at 50 °C for 2.5 min. Similar behavior can be observed in the four-arm PEOs, wherein the long period increases from 15.0 to 18.2 nm.

The heating event clearly involves a thickening process of the original crystals grown at 32 °C, which may be achieved by cooperative motion of the arms and coupling agents. However, this thickening process can only be achieved when the temperature exceeds 44 °C, indicating the large-scale cooperation motion is forbidden at temperatures below 44 °C.[21,22] This implies that the thickening is an activated process, which is associated with the small endotherm (near 44 °C) found on the DSC melting trace for the star PEOs crystallized at T_c < 40 °C. Furthermore, it is worth noting that since the thickening starts at 44 °C, the T_m's of the crystals grown at T_c < 36 °C observed in DSC (Figures 12 and 13) should be representative of already thickened crystals during heating.

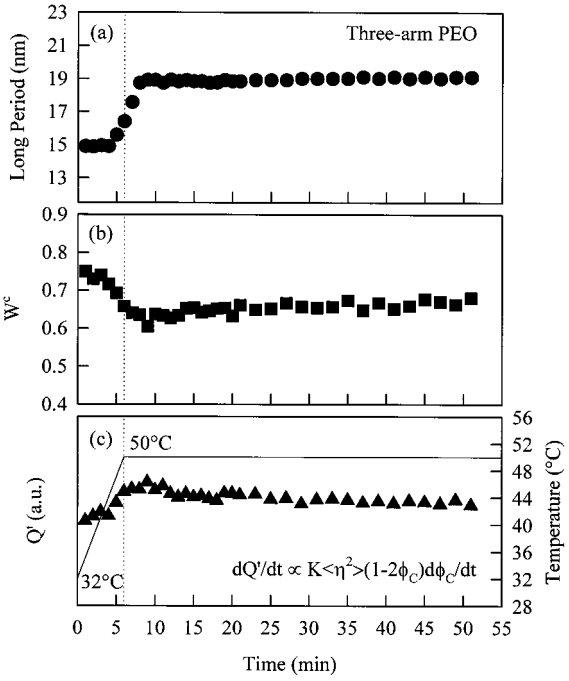

Figure 14. Synchrotron WAXD and SAXS results of the heating and annealing of the three-arm star PEO crystallized at 32 °C followed by annealing at 50 °C for various t_a's: (a) change of long period, (b) change of crystallinity, and (c) change of the relative invariant Q'. The solid line in part c represents the temperature profile.

Figure 14b,c illustrates the changes in crystallinity and relative invariant Q' in this simultaneous experiment. The crystallinity initially remains constant at 0.75 before it starts to (as the long period starts to increase) drop at 44 °C. The crystallinity is 0.64 after 50 °C is reached for 2.5 min, indicating a partial crystal melting. This is followed by a slow increase, revealing a recrystallization process. The development of the relative invariant Q' with time can be recognized as a two-step process: an initial Q' increase during heating reaching a maximum once held at 50 °C for 2.5 min, followed by a continuous but gentle decrease. Therefore, the time at which minimum crystallinity and maximum Q' are realized corresponds to that of reaching a long period of 19.0 nm.

The explanation of the Q' changes with time during the annealing requires further discussion. The Q' obtained by the integration of q from 0.08 to 0.2 nm^{-1} is the major contribution of the invariant Q in this research. Therefore,

$$Q' \approx Q \propto K\langle\eta^2\rangle\phi_c(1-\phi_c) \qquad (3)$$

where K is a constant, $\langle\eta^2\rangle$ is the mean square of the electron density difference between the crystalline and amorphous polymer, and ϕ_c is the volume crystallinity. The first derivative of Q' with respect to time can be obtained:

$$dQ'/dt \propto K\langle\eta^2\rangle(1 - 2\phi_c)\, d\phi_c/dt \quad (4)$$

On the basis of the WAXD results (Figure 14b), the weight crystallinity (and therefore, ϕ_c) of the three-arm PEO is always higher than 0.5 during heating and annealing. This gives rise to a negative $(1 - 2\phi_c)$ term in eq 4. During heating from 44 to 50 °C, Q' in eq 3 increases (Figure 14c), and thus, dQ'/dt in eq 4 is positive, which requires that $d\phi_c/dt$ in eq 4 be negative, i.e., a decrease in the volume crystallinity with respect to time. It can be concluded that in this heating process the long period increase is mainly attributed to a partial crystal melting which increases the thickness of the amorphous layer. After Q' reaches a maximum, it gradually decreases during isothermal annealing while the long period remains nearly constant. The decrease in Q' (Figure 14c) results in a negative dQ'/dt in eq 4, which makes $d\phi_c/dt$ positive. This is confirmed by WAXD results (Figure 14b). Therefore, the crystal lamellar thickness increases at the cost of a reduction of the amorphous layer thickness. A similar observation is also made in the four-arm PEO.

The annealing process can substantially change the thermodynamic stability and morphology of three- and four-arm PEO crystals with irregular conformation formed at high ΔT's. The annealed three-arm PEO crystals possess a T_m of 56.8 °C and a long period of 19.0 nm, which are almost identical to the values of 57.0 °C and 19.1 nm for the three-arm PEO crystal grown directly at 48 °C. In the case of the four-arm PEO, although the annealing process improves the thermodynamic stability of the sample crystallized at high ΔT, the annealed crystals still remain in a state with a lower T_m and thinner long period compared to those grown directly from the melt at high T_c. The melting temperature of 57.1 °C for the annealed four-arm PEO crystals is 1.0 °C lower than that for four-arm PEOs crystallized at 48 °C (58.1 °C). Furthermore, a long period of 18.2 nm for the annealed crystal is approximately 1.0 nm thinner than that of 19.2 nm for the crystal formed at 48 °C. This phenomenon indicates that the changing of the irregular conformation in four-arm PEO crystals is more difficult to achieve by annealing compared with the three-arm PEOs. It is conceivable that in the four-arm PEO four arms of each molecule are required to move simultaneously during annealing, and thus, the cooperative motion becomes more restricted; therefore, the irregular conformation cannot fully adjust.

Conclusion

The crystallization behaviors of the star PEOs having three- and four-arms with equal arm lengths (M_a = 2220) have been monitored by simultaneous WAXD and SAXS experiments. It has been found that in addition to the T_c dependence, overall crystallization rates are critically associated the number of arms. In the initial stage of crystallization, an apparent thinning process that depends upon the T_c can be found. This may be explained by the self-seeding effect at low ΔT's, the coupling agent arrangements, and the crystallinity maximization at intermediate ΔT's. This thinning process ceases at high ΔT's. After complete crystallization, the final long periods of these star PEOs crystallized at low ΔT's attain a value that corresponds to the contributions of crystalline PEO lamellae, both of the coupling agents, and the uncrystallized PEO arms. The T_m's of these crystals show T_c dependency, in particular, in a T_c range between 36 and 44 °C. These observations are remarkably similar to the long period changes with T_c. Overall, the star PEO crystals exhibit T_m's corresponding to the lamellar crystals having a thickness of the single arm length. Annealing experiments indicate that the star PEO crystals grown at high ΔT's may be annealed through a partial crystal melting and recrystallization at higher temperatures. However, the four-arm PEO crystals are more difficult to anneal compared with the three-arm PEO crystals under the same annealing conditions. This is possibly due to the restricted motion among the four arms.

Acknowledgment. This research was supported by the National Science Foundation (DMR-9617030). Research was carried out in part at the National Synchrotron Light Source (Beam X-27C) at Brookhaven National Laboratories, which is supported by the U.S. Department of Energy, Division of Material Science and Division of Chemical Sciences.

References and Notes

(1) Arlie, J. P.; Spegt, P. A.; Skoulios, A. E. *Makromol. Chem.* **1966**, *99*, 170.
(2) Arlie, J. P.; Spegt, P. A.; Skoulios, A. E. *Makromol. Chem.* **1967**, *104*, 212.
(3) Spegt, P. *Makromol. Chem.* **1970**, *139*, 139.
(4) Galin, J.-C.; Spegt, P.; Suzuki, S.; Skoulios, A. E. *Makromol. Chem.* **1974**, *175*, 991.
(5) Thierry, A.; Skoulios, A. E. *Colloid Polym. Sci.* **1977**, *255*, 334.
(6) Thierry, A.; Skoulios, A. E. *Eup. Polym. J.* **1977**, *13*, 169.
(7) Kovacs, A. J.; Gonthier, A. *Colloid Polym. Sci.* **1972**, *250*, 530.
(8) Kovacs, A. J.; Gonthier, A.; Straupe, C. *J. Polym. Sci., Polym. Symp.* **1975**, *50*, 283.
(9) Kovacs, A. J.; Straupe, C.; Gonthier, A. *J. Polym. Sci., Polym. Symp.* **1977**, *59*, 31.
(10) Kovacs, A. J.; Straupe, C. *J. Crystal Growth* **1980**, *48*, 210.
(11) Kovacs, A. J.; Straupe, C. *Faraday Discuss. Chem. Soc.* **1979**, *68*, 225.
(12) Cheng, S. Z. D.; Zhang, A.-Q.; Chen, J.-H. *J. Polym. Sci., Polym. Lett.* **1990**, *28*, 233.
(13) Cheng, S. Z. D.; Zhang, A.-Q.; Chen, J.-H.; Heberer, D. P. *J. Polym. Sci., Polym. Phys. Ed.* **1991**, *29*, 289.
(14) Cheng, S. Z. D.; Chen, J.-H.; Zhang, A.-Q.; Heberer, D. P. *J. Polym. Sci., Polym. Phys. Ed.* **1991**, *29*, 299.
(15) Cheng, S. Z. D.; Chen, J.-H. *J. Polym. Sci., Polym. Phys. Ed.* **1991**, *29*, 311.
(16) Cheng, S. Z. D.; Zhang, A.-Q.; Barley, J. S.; Chen, J.-H.; Habenschuss, A.; Zschack, P. R. *Macromolecules* **1991**, *24*, 3937.
(17) Cheng, S. Z. D.; Chen, J.-H.; Zhang, A.-Q.; Barley, J. S.; Habenschuss, A.; Zschack, P. R. *Polymer* **1992**, *33*, 1140.
(18) Cheng, S. Z. D.; Chen, J.-H.; Zhang, A.-Q.; Barley, J. S.; Habenschuss, A.; Zschack, P. R. *Macromolecules* **1992**, *25*, 1453.
(19) Cheng, S. Z. D.; Wu, S. S.; Chen, J.-H.; Zhuo, Q.; Quirk, R. P.; von Meerwall, E. D.; Hsiao, B. S.; Habenschuss, A.; Zschack, P. R. *Macromolecules* **1993**, *26*, 5105.
(20) Lee, S. W.; Chen, E. Q.; Zhang, A.; Yoon, Y. C.; Moon, B. S.; Lee, S. K.; Harris, F. W.; Cheng, S. Z. D.; von Meerwall, E. D.; Hsiao, B. S.; Verma, R.; Lando, J. B. *Macromolecules* **1996**, *29*, 8816.
(21) Chen, E.-Q.; Lee, S.-W.; Zhang, A.; Moon, B. S.; Lee, S.; Harris, F. W.; Cheng, S. Z. D.; Hsiao, B. S.; Yei, F. *Polymer* **1999**, *40*, 4543−4551.
(22) Chen, E.-Q.; Lee, S.-W.; Zhang, A.; Moon, B. S.; Lee, S.; Harris, F. W.; Cheng, S. Z. D.; Hsiao, B. S.; Yei, F.; von Meerwall, E. D. In *Scattering from Polymers*; ACS Symposium Book Series; American Chemical Society: Washington, DC, in press.
(23) Keller, A.; Cheng, S. Z. D. *Polymer* **1998**, *39*, 4461.
(24) Cheng, S. Z. D.; Keller, A. *Annu. Rev. Mater. Sci.* **1998**, *28*, 553.
(25) von Meerwall, E. D. *Adv. Polym. Sci.* **1983**, *54*, 1; *Rubber Chem. Technol.* **1985**, *58*, 527.

(26) Chu, B.; Harney, P. J.; Li, Y.; Linliu, K.; Yeh, F.; Hsiao, B. S. *Rev. Sci. Instrum.* **1994**, *65* (3), 597.
(27) Ryan, A. J.; Stanford, J. L.; Bras, W.; Nye, T. M. W. *Polymer* **1997**, *38*, 759.
(28) Orofino, T. A. *Polymer* **1961**, *2*, 295.
(29) Orofino, T. A. *Polymer* **1961**, *2*, 305.
(30) Takahashi, Y.; Tadokoro, H. *Macromolecules* **1973**, *6*, 672.
(31) Cheng, S. Z. D.; Barley, J. S.; von Meerwall, E. D. *J. Polym. Sci., Polym. Phys. Ed.* **1991**, *29*, 515.
(32) Hoffman, J. D.; Davis, G. T.; Lauritzen, J. I., Jr. In *Treatise on Solid State Chemistry*; Hannay, N. B., Ed.; Plenum: New York, 1976; Vol. 3, Chapter 7, pp 497−614.
(33) Hoffman, J. D. *Polymer* **1982**, *23*, 656; **1983**, *24*, 3.
(34) Hoffman, J. D.; Miller, R. L. *Macromolecules* **1988**, *21*, 3038.
(35) Hoffman, J. D. *Macromolecules* **1986**, *19*, 1124.
(36) Hoffman, J. D.; Miller, R. L. *Polymer* **1997**, *38*, 3151.

MA9900176